Materials Letters 92 (2013) 86–89

Contents lists available at SciVerse ScienceDirect

Materials Letters

journal homepage: www.elsevier.com/locate/matlet

Effect of densification mechanism on the $\Sigma 2$ grain boundary plane distribution in WC–Co composites

Xiaokun Yuan [a], Xiaoyan Song [a], Harry Chien [b], Jia Li [b], Gregory S. Rohrer [b,*]

[a] College of Materials Science and Engineering, Beijing University of Technology, Beijing 100124, China
[b] Department of Materials Science and Engineering, Carnegie Mellon University, Pittsburgh, PA 15213-3890, USA

ARTICLE INFO

Article history:
Received 6 September 2012
Accepted 17 October 2012
Available online 26 October 2012

Keywords:
Grain boundary
Cemented carbide
Sintering
Electron microscopy
Five parameter analysis

ABSTRACT

The effect of the densification mechanism on the $\Sigma 2$ grain boundary plane distribution was investigated in WC–Co composites. Specimens were prepared separately by sintering in hot isostatic press (sinter-HIP) and spark plasma sintering (SPS). It was found that the $\Sigma 2$ twist boundary is the most common boundary in both cases, but that the SPS material had more than three times the relative area of these boundaries compared to the sinter-HIP material. Measurements of the WC/WC and WC/Co boundary lengths are compared to measured mechanical properties and found to be consistent with established stereological results, suggesting a path to link interface area measurements to the mechanical properties of WC–Co samples.

1. Introduction

The mesoscale grain boundary network structure influences the integrity and performance of polycrystalline materials [1]. WC–Co composites are important engineering materials widely used for their hardness and abrasion resistance. Among carbide/carbide boundaries, the $\Sigma 2$ grain boundary occurs most frequently and can be described as a 90° rotation around the [10–10] axis [2]. Note that in the hexagonal WC structure, the *c* and *a* lattice parameters differ by only 2%, so the $\Sigma 2$ boundary can be taken as an "approximate" coincidence site lattice (CSL) boundary. While this is not a true CSL boundary in the conventional sense, for consistency with the previous literature we refer to it in this paper as a $\Sigma 2$ grain boundary [2].

In the present work, a stereological approach named "five parameter analysis (FPA)" is deployed to measure the grain boundary plane distributions (GBPD) from electron backscattered diffraction (EBSD) data. The GBPD is expressed in terms of five macroscopically observable parameters, including three Eulerian angles to describe the lattice misorientation across the boundary, and two spherical angles to describe the orientation of the grain boundary plane normal. There are increasing studies about the $\Sigma 2$ boundary distribution using EBSD [3,4] and the FPA method [5,6]. However, because of the difficulty of obtaining the very large data sets needed to apply the FPA method to a hexagonal material, it has not previously been possible to compare the GBPDs of WC–Co samples prepared in different ways.

Accordingly, the objective of the current work is to use the FPA method to calculate and compare the GBPDs from similar materials that differ only in their densification mechanism. The results will show how the densification mechanism affects the GBPD of $\Sigma 2$ boundaries. Moreover, the variations in the lengths of WC/WC and WC/Co interfaces per area are compared to variations in the measured mechanical properties of the WC–Co composites.

2. Experimental

The two cemented carbide samples were prepared from WC–Co composite powder with a cobalt fraction of 8 wt% and with no intentional alloying additions. Sample 1 (similarly hereinafter) was prepared by sintering in hot isostatic press (sinter-HIP) in a 6 MPa argon atmosphere with a sintering temperature of 1500 °C, just above the melting point of Co, was maintained for 30 min. Sample 2 (similarly hereinafter) was prepared via spark plasma sintering (SPS) process under an applied pressure of 50 MPa with a sintering temperature of 1200 °C maintained for 5 min.

Samples were polished and then etched in Murakami's reagent for 5 s before EBSD analysis. The EBSD measurements were performed using a high speed Hikiari camera (EDAX, Inc., USA) incorporated in a Quanta 200 field emission environmental scanning electron microscope (FEI Company, USA). On each sample, more than 2×10^5 grain boundary traces were recorded to achieve acceptable statistics for the GBPD calculation.

The microtexture and misorientation statistics represented by the boundary length fraction were derived from TSL OIM Analysis 5.3 software (EDAX Inc., USA). In this analysis, all of the interfaces in the EBSD maps are approximated by individual line segments. The complete set of interface line segments was divided into two

* Correspondence author. Tel.: +1 412 268 2696; fax: +1 412 268 3113.
E-mail address: gr20@andrew.cmu.edu (G.S. Rohrer).

0167-577X/$ - see front matter © 2012 Elsevier B.V. All rights reserved.
http://dx.doi.org/10.1016/j.matlet.2012.10.074

sets for separate analysis; one set contained only WC/WC grain boundaries and the other contained WC/Co interfaces. The GBPDs for the $\Sigma 2$ boundaries were calculated using programs developed at Carnegie Mellon University. The programs use a stereological procedure described in reference [7]. Using the FPA method, the grain boundary distribution, $\lambda(\Delta g, n)$, is defined as the relative areas of grain boundaries with a misorientation, Δg, and boundary plane normal, n, in units of multiples of a random distribution (MRD).

3. Results and discussion

The microstructures of two samples are depicted by the image quality (IQ) maps in Fig. 1, with $\Sigma 2$ boundaries highlighted in red. IQ maps represent the quality of EBSD patterns, which is lower for points near grain boundaries. Both samples exhibit a continuous skeleton of prismatic WC grains embedded in the cobalt binder phase. However, the mean grain size of WC in sample 1 (about 1 μm) are larger than in sample 2 (about 0.5 μm). The difference in the grain size is caused by the different densification mechanisms. Sample 1 is prepared by the sinter-HIP process, and there is rapid grain growth accomplished by coalescence of WC grains [8] during both the heat up and isothermal hold at the liquid phase sintering temperatures [4]. Sample 2 is prepared by the SPS process, which is performed with a reduced sintering temperature and a much shorter holding time, and grain growth is effectively inhibited during the sintering [9]. Therefore, sample 2 has a finer grain structure as compared with sample 1.

The FPA method is carried out by examining two dimensional sections of the five parameter grain boundary character distribution (GBCD), and thus is possible to compare the grain boundary plane distribution at specific misorientations. The misorientation angle distribution was calculated to analyze the orientation relationship between WC grains. Both samples showed two misorientation angle preferences, corresponding to the sharp peaks at 30 and 90 degree. Moreover, to examine the distribution of misorientation axes, the data were plotted in axis–angle space, to further resolve the orientation relationship between WC grains. In both samples, there is a strong peak at the [10–10] rotation axis, indicating that [10–10] is the dominant misorientation axis, and boundaries with such misorientations occur most frequently. The relative areas of grain boundary planes can be plotted on a stereographic projection for the misorientations where maxima occur in the distribution. For example, Fig. 2 shows the relative areas of different grain boundary planes at the misorientation of 90° about [10–10]. For both samples, the maximum of the distribution is at the position corresponding to the misorientation axis [10–10], indexed as an oval, which means the boundary plane is perpendicular to the common rotation axis of the grain pair on the two sides; thus, it is a twist configuration. The absence of boundaries along the great circle perpendicular to the misorientation axis (that passes through the (0001) position, indexed as

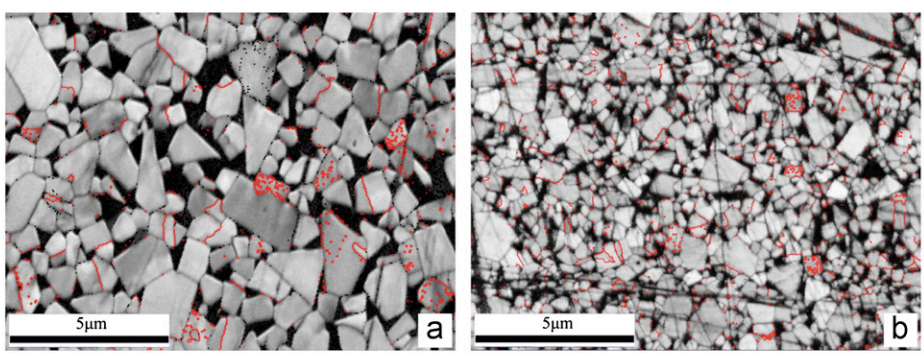

Fig. 1. Image quality maps for WC–Co specimens, with $\Sigma 2$ boundaries highlighted in red, (a) sample 1 and (b) sample 2. (For interpretation of the reference to color in this figure legend, the reader is referred to the web version of this article.)

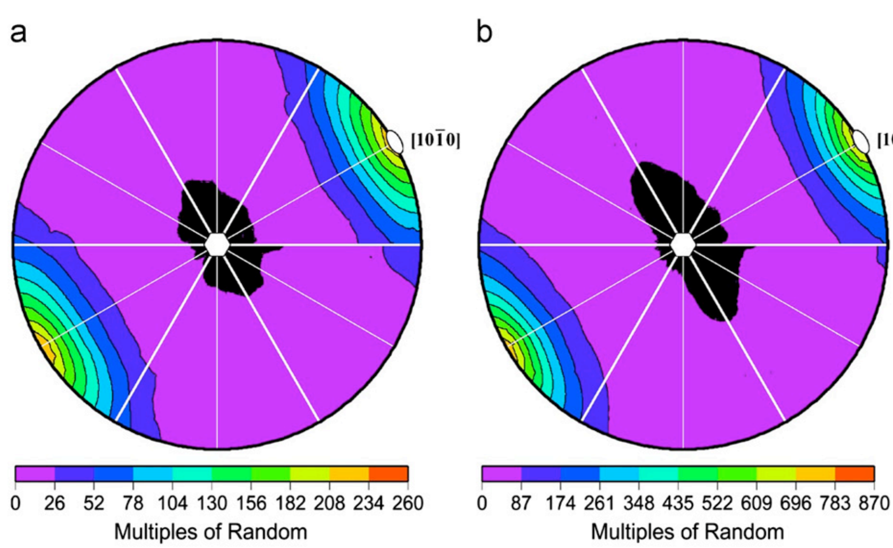

Fig. 2. Grain boundary plane distributions for the $\Sigma 2$ in WC–Co specimens, (a) sample 1 and (b) sample 2.

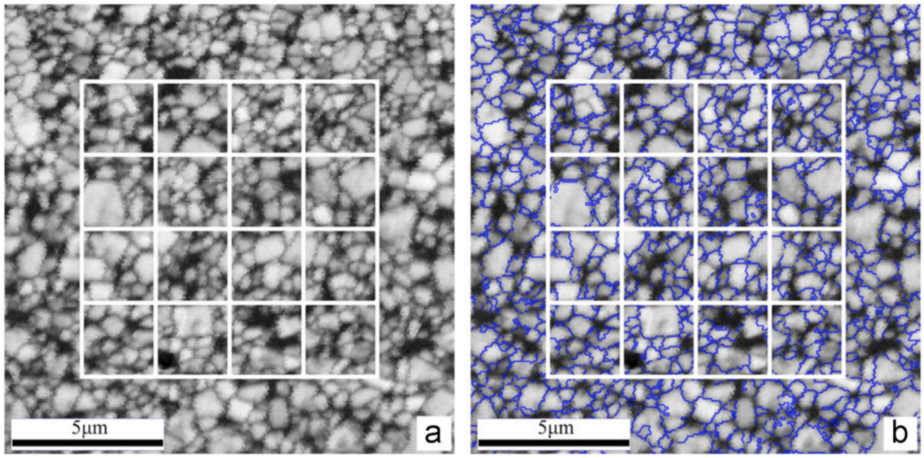

Fig. 3. Prerequisites for stereological method, with an IQ map as background, (a) using an equidistanced lattice for counting stereological parameters and (b) general WC/WC boundaries (in blue) are evenly distributed. (For interpretation of the reference to color in this figure, the reader is referred to the web version of this article.)

Table 1
Properties of WC–Co specimens.

	Sample 1	Sample 2
WC/WC boundary number/μm^2	2.65	4.72
WC/Co boundary number/μm^2	3.87	7.85
Vickers hardness (kg/mm^2)	1350	1873
Fracture toughness (MPa m$^{1/2}$)	16.46	12.09

a hexagon) indicates that tilt boundaries are not common at this misorientation. Note that while the shapes of the distributions are the same, the relative areas of $\Sigma 2$ twist boundaries in sample 1 (260 MRD) and sample 2 (870 MRD) indicate that the SPS processed sample has a higher $\Sigma 2$ boundary population than the sinter-HIP processed sample by a factor of about 3.4.

The difference in the $\Sigma 2$ grain boundary area in the two samples suggests that they were not in equilibrium. A recent theory for the development of anisotropic GBPDs suggests that in the late stages of microstructural development, the relative areas will reach a steady state [10]. Based on the samples here, it appears that the concentration of $\Sigma 2$ grain boundaries decreases with grain size. A similar conclusion was reached through an analysis of the misorientation distributions of multiple samples [4].

The present measurements of interface length are interesting to consider in the context of a recently developed stereological method that quantitatively relates observations of the WC mean grain size (d_{WC}) and Co mean free path (L_{Co}) to the hardness and fracture toughness [11]. According to Ref. [11], Vickers hardness has a positive linear relationship with $d_{WC}^{-1/2}$ or $L_{Co}^{-1/2}$, and fracture toughness has an opposite trend. In the current work, we have measurements of the WC/WC grain boundary length, which can serve as a proxy for d_{WC} and the WC/Co phase boundary length, which can serve as a proxy for L_{Co}. The prerequisites for using these quantities are that the WC and cobalt phases are evenly distributed (as shown in Fig. 3). However, note that when we measure these interface lengths on a per area basis, as illustrated schematically in Fig. 3, then an increase in the WC/WC boundary length per area means a decrease in the WC mean grain size and an increase in WC/Co boundary length per area decreases the Co mean free path. This means that the hardness should increase with WC/WC boundary length and the WC/Co interface length and the fracture toughness should decrease. These trends are revealed by the measurements shown in Table 1, which shows that the sample with larger interface length per area has a greater hardness and lower toughness.

4. Conclusions

Five parameter analysis found that WC/Co samples produced by the SPS process have more than three times the relative area of $\Sigma 2$ boundaries than samples produced by the sinter-HIP process and that the $\Sigma 2$ twist boundary is the most common boundary in both cases. When the areal density of interfacial segments increases, the hardness increases and fracture toughness decreases. This is consistent with the results of conventional stereology and suggests that WC/WC grain boundary area and WC/Co interface area can be used as proxies for the WC grain size and Co mean free path to develop structure–property relationships.

Acknowledgments

GSR acknowledges support from the Office of Naval Research Grant N00014-11-1-0678. Facilities support from the Carnegie Mellon MRSEC, under National Science Foundation under Award Number DMR-0520425, are also acknowledged. The work is also supported by (China) the Beijing Natural Science Foundation 2123061.

References

[1] Rohrer GS. Measuring and interpreting the structure of grain-boundary network. J Am Ceram Soc 2011;94:633–46.
[2] Hagege S, Nouet G, Delavignette P. Grain boundary analysis in TEM (IV): Coincidence and the associated defect structure in tungsten carbide. Phys Status Solidi A 1980;62:97–107.
[3] Ostberg G, Farooq MU, Christensen M, Andren HO, Klement U, Wahnstrom G. Effect of $\Sigma 2$ grain boundaries on plastic deformation of WC-Co cemented carbides. Mater Sci Eng A 2006;416:119–25.
[4] Kumar V, Fang ZZ, Wright SI. An analysis of grain boundaries and grain growth in cemented tungsten carbide using orientation imaging microscopy. Metall Mater Trans A 2006;37:599–607.
[5] Kim CS, Rohrer GS. Geometric and crystal—the work described is about the effect of densification mechanism on the $\Sigma 2$ grain boundary plane distribution in WC–Co composites graphic characterization of WC surfaces and grain boundaries in WC–Co composites. Interface Sci 2004;12:19–27.
[6] Kim CS, Massa TR, Rohrer GS. Interface character distributions in WC–Co composites. J Am Ceram Soc 2008;91:996–1001.

[7] Saylor DM, Dasher BE, Adams BL, Rohrer GS. Measuring the five-parameter grain-boundary distribution from observations of planar sections. Metall Mater Trans A 2004;35:1981–9.
[8] Fang Z, Eason JW. Study of nanostructured WC–Co composites. Int J Refract Met Hard Mater 1995;5:297–303.
[9] Zhao SX, Song XY, Wei CB, Zhang L, Liu XM, Zhang JX. Effects of WC particle size on densification and properties of spark plasma sintered WC–Co cermet. Int J Refract Met Hard Mater 2009;27:1014–8.
[10] Dillon SJ, Rohrer GS. Mechanism for the development of anisotropic grain boundary character distributions during normal grain growth. Acta Mater 2009;57:1–7.
[11] Zhao SX, Song XY, Liu XM, Wei CB, Wang HB, Gao Y. Quantitative relationships between microstructure parameters and mechanical properties of ultrafine cemented carbides. Acta Metall Sin 2011;47:1188–94.